J/ψ production measurement in $p+p$ and nucleus-nucleus collisions at $\sqrt{s_{\rm NN}} = 200$ GeV by the PHENIX experiment at the Relativistic Heavy Ion Collider

Alberto Baldisseri, Hervé Borel, Javier Castillo, Mercedes Castillo, Jean-Luc Charvet, Jean Gosset, Hugo Pereira Da Costa, Catherine Silvestre Tello, Florent Staley

June 23, 2008

1 Introduction

The PHENIX experiment is located on the Relativistic Heavy Ion Collider (RHIC) at the Brookhaven National Laboratory (BNL). It aims to study the properties of nuclear matter under high pressure and high temperature conditions and identify the possible formation of a Quark-Gluon Plasma (QGP), a state where the quarks and gluons are deconfined and can evolve quasi-freely on distances larger than the nucleon size.

Many probes are measured using the PHENIX apparatus to study the properties of the created medium in relativistic nucleus-nucleus collisions and notably the production of the J/ψ resonance which is a heavy quarkonium consisting of a charm and anti-charm ($c\overline{c}$) pair. The suppression of the J/ψ production with growing energy density of the medium is considered a promising proof of the formation of the QGP because of the inability for the charm quark pairs to form a bound state if the colour density of the surrounding medium is large enough to screen the interaction between the two quarks [1]. PHENIX can measure J/ψ at mid rapidity ($|y| < 0.35$) via its decay in two electrons and at forward rapidity ($|y| \in [1.2, 2.2]$) via its decay in two muons.

The DAPNIA joined the PHENIX experiment in 2001 and financed 25 % of the readout electronics of one PHENIX muon arm spectrometer. Our group contributed to all data taking periods from 2003 to 2007 covering $p+p$, d + Au, Au + Au and Cu + Cu collisions. For all the corresponding analysis, the group focused on measuring the J/ψ production at forward rapidity. In 2004, we took the responsibility of the software used to reconstruct the trajectory and momentum of the particles (mostly muons) at forward rapidity. In 2006 we implemented an offline alignment procedure that is more precise and automated than the one used in the past. This method has been applied to the 2006 muon tracker alignment prior to the data reconstruction. Starting from 2007 we now also assume the coordination of all PHENIX simulations.

We briefly describe here the PHENIX muon spectrometers and the corresponding track reconstruction software. We then report PHENIX main results on J/ψ production in $p+p$ and nucleus-nucleus collisions at a center of mass energy per nucleon-nucleon collision $\sqrt{s_{\rm NN}} = 200$ GeV.

2 The Quark-Gluon Plasma in relativistic heavy ion collisions

The QGP is predicted by lattice Quantum Chromodynamics (QCD) calculations to be formed above a temperature of order $T_c = 170$ MeV for a baryon chemical potential (related to the difference between the baryonic and anti-baryonic density in the medium) $\mu_b = 0$ [2]. Such a temperature is expected to be achieved in ultra-relativistic heavy ion collisions if the center of mass energy per nucleon-nucleon collision is high enough and if the collisions are central enough. The collision centrality characterizes the distance between the centers of the two colliding nuclei (also called impact parameter). Most central collisions correspond to an impact parameter b close to zero. Apart from b, other variables are used to describe the collision centrality:

- the number of participant nucleons $N_{\rm part}$ which is the number of nucleons in the colliding nuclei that interact (as opposed to spectator nucleons that remain unaffected). For a peripheral collision $N_{\rm part} = 2$. It increases when the collision is more central.
- the number of equivalent nucleon-nucleon collisions $N_{\rm coll}$. For a peripheral collision $N_{\rm coll} = 1$. It increases when the collision is more central.

To identify the formation of a QGP in nucleus-nucleus (A+A) collisions, each measurement is compared to a reference obtained at the same energy in $p+p$ collisions. Some nuclear effects that do not involve the formation of the QGP occur in A+A collisions that are not present in $p+p$ collisions. To evaluate such effects an additional test measurement is performed in $p+\mathrm{A}$ (or for RHIC $\mathrm{d}+\mathrm{A}$) collisions, for which no QGP is formed.

3 The PHENIX spectrometer

Figure 1 shows a schematic view of the PHENIX apparatus. It consists in a central arm which measures particles emitted at mid rapidity ($|y| < 0.35$) and two muon arms which measure particles emitted at forward rapidity ($|y| \in [1.2, 2.2]$). The PHENIX central arm has very good particle identification and measures hadrons, photons and electrons at a momentum $p > 0.2$ GeV/c. Its azimuthal coverage is $\Delta\Phi = \pi$. The PHENIX muon arms are placed behind two front absorbers located on both sides of the interaction point that stop most hadrons produced during the collision. They measure principally muons at a momentum $p > 2$ GeV/c and have full azimuthal coverage.

Additional detectors are used to determine the collision centrality (in the case of nucleus-nucleus collisions) and the position of the collision along the beam axis. They are the Beam-Beam counters (BB) and the Zero Degree calorimeters (ZDC).

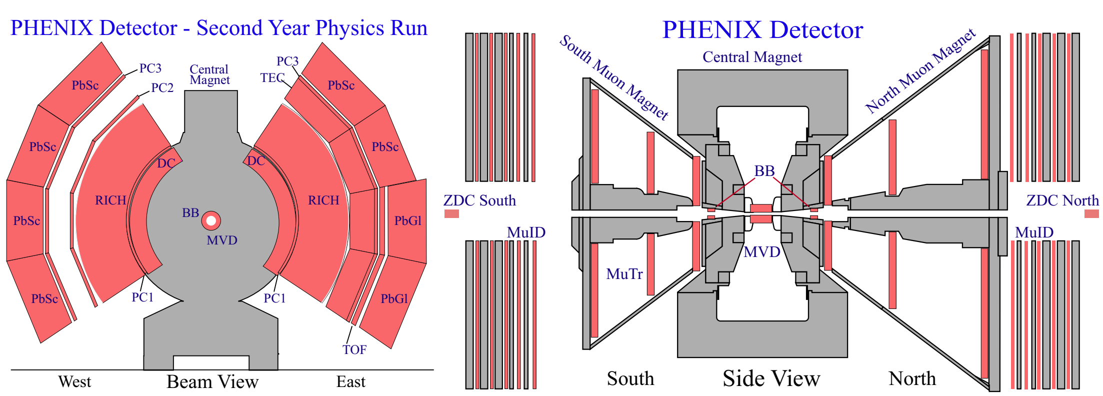

(a) front view

(b) side view

Figure 1: Schematic view of the PHENIX spectrometer

A more complete description of the PHENIX apparatus is found in [3]. The muon arms are described in more detail in the next section.

4 The muon spectrometers

4.1 Detector

Each PHENIX muon arm consists of two parts: the muon identifier (MuID) and the muon tracker (MuTR).

The MuID consists of five alternating layers of steel absorbers and detection planes. Each detection plane consists of two layers of horizontal and vertical Iarrocci tubes. It is segmented in six panels, located around the beam. One MuID plane and its constituting panels is shown in Figure 2(a). The MuID is used to trigger on muons (as opposed to hadrons) that have a high enough momentum to penetrate the steel absorber layers.

The MuTR consists of three stations of Cathode Strip Chambers. The first and second stations have three chambers each and the third station has two chambers. Each chamber is segmented into eight octants that are in turn divided into two half octants as shown in Figure 2(b). For each half octant, the cathodes are segmented into strips of width $w = 0.5$ cm and with a spacing of 1 cm. The strips of the two cathodes have slightly different orientations, close to the radial direction r, to allow 2D reconstruction. The read-out electronics is plugged at the end of each strip and consists of analog-to-digital converters (ADC). The high voltage is applied on the anode wires which are oriented in the direction perpendicular r. The MuTR resides in a radial magnetic field that is created by a solenoidal magnet located around the beam and field closure plates located outside of the detector acceptance. The MuTR is used to measure the particles trajectory and momentum. A precise muon identification can be performed offline by matching the particle momentum measured in the MuTR with the particle penetration depth in the MuID.

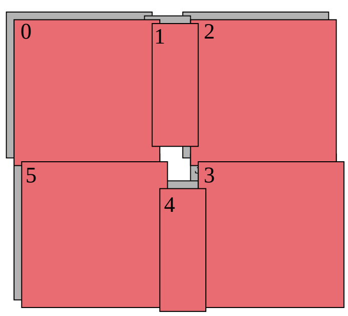

(a)

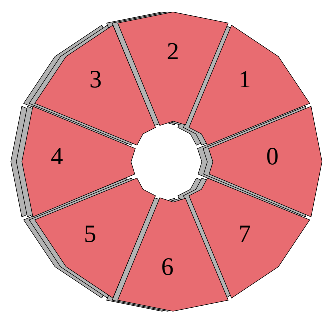

(b)

Figure 2: Schematic view of one PHENIX muon identifier detection plane (left) and one muon tracker station (right). See text for details.

The DAPNIA hardware contribution to the PHENIX spectrometer was to finance and maintain the read-out electronics of one of the muon arms in association with several teams of the IN2P3 inside the PHENIX-France collaboration. These teams also took the responsibility of building this electronics.

The maintenance of the readout electronics consists mostly in replacing faulty modules between data taking periods; making sure that the Muon Tracker is ready for data taking before each new period and checking the well functioning of the detector during data taking. This includes checking the daily calibrations taken by the shift crew, taking note of the tripped high voltage channels and faulty read-out electronic modules to recover them as soon as possible and monitoring the quality of the data offline. This responsibility was carried over by our group during portions of each data taking period since 2003 on top of the regular shift duties assigned to all PHENIX collaborators.

4.2 Track reconstruction software

Object oriented software is used offline to reconstruct the trajectory and momentum of the particles passing through the muon arms from the hits in the detector. The reconstruction algorithm first looks for straight segments of tracks in the MuID (where no magnetic field is present) and uses these segments as seeds for the tracking in the MuTR. Each seed is used to find one matching space point and the corresponding track direction in the MuTR station 3. Both are extrapolated to station 2, accounting for the magnetic field and using an approximate particle momentum estimated with a bend-plane fitting technique. Hits from the station 2 are added to the track and the momentum estimate is re-evaluated. A second extrapolation is then performed towards station 1 and the corresponding hits are also added. The track is then fitted using a Kalman filter technique to get the most precise estimate of the particle charge, position and momentum, using all available information. It is then extrapolated backward through the front absorber with proper accounting for the particle energy loss and propagation of the particle multiple scattering to the track parameters error. To identify J/ψ, all possible pairs of reconstructed particles are formed. Each pair is fitted together with the vertex z position measured by the Beam Beam counters and the pair invariant mass is calculated.

Starting from 2003, the muon arms track reconstruction software was entirely rewritten to better suit the requirements of the 2004 Au + Au run for which the number of particles per event and thus the constraints in terms of reconstruction time and efficiency were larger than for the previous data taking periods. In 2004, the group took the responsibility of maintaining and improving this software, as it was officially adopted by the PHENIX collaboration in place of the one used for the previous analysis.

4.3 Detector alignment

The efficiency of the track reconstruction algorithm depends notably on the precise knowledge of the position of the detectors constituting the spectrometer. To achieve maximum accuracy, an offline alignment procedure is used to provide corrections to the expected position of the detectors (from the initial survey of the spectrometer) so that they match their true position. These corrections are optimum when the distribution of the residuals in each detector (difference between the hit position and the position of the corresponding fitted track) is centered on zero and has a minimum width. This was originally achieved iteratively by assuming that the position of a given set of detectors was perfectly known, using these detectors as a reference to reconstruct the tracks, modifying the alignment corrections of the remaining detectors to center their corresponding residual distributions on zero and changing the set of reference detectors for the second and subsequent iterations. Such a method is time consuming since the full reconstruction of the tracks has to be performed at each iteration; it uses only part of the information (namely the average values of the residual distributions) and it is not guaranteed to converge.

Starting from 2006 an alternative alignment procedure was developed by our group that relies on the simultaneous minimization of the chi-square of many tracks, as a function of both the track parameters and the track independent detector alignment parameters. With such a procedure only a limited (and smaller) set of detectors are used as reference in order to avoid global transformations of the spectrometer that would leave the tracks chi-square unchanged. Moreover, the minimization of the chi-square provides the optimum set of alignment corrections without the need for iterations.

This so called global procedure was applied to 2003 data and compared to the existing set of alignment corrections. The result is illustrated in Figure 3 which shows the mean value of the residual distributions in each half-octant of the MuTR as a function of the detector index for three different sets of corrections: without corrections (triangle), with the old corrections (circles) and with the new corrections (squares). The mean values are on average better centered on zero when using the new set of alignment corrections. These new corrections are used for the reconstruction of the 2006 data and the global alignment procedure will be officially used for PHENIX future data taking periods.

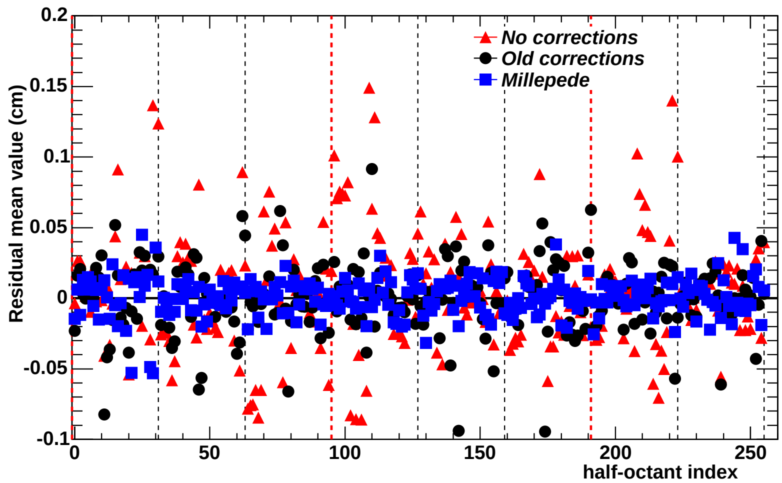

Figure 3: Mean value of the residual distribution in each half-octant of the MuTR as a function of the detector index for three sets of alignment corrections. Triangles correspond to no alignment corrections; circles to the corrections obtained using the iterative method and squares to the corrections obtained with the global alignment procedure.

5 J/ψ measurements

J/ψ are measured in the central spectrometer via their decay in two electrons and in the muon spectrometer via their decay in two muons. The invariant mass distribution of di-lepton pairs of opposite sign is formed and the combinatorial background constituted by pairs of uncorrelated leptons is subtracted using an event-mixing technique (that is, by forming the invariant mass distribution of leptons that do not belong to the same event). The event mixed background is normalized to the physical distribution by using pairs of leptons that have the same sign. The background subtracted distribution is fitted by several line shapes that account for both the J/ψ signal (via either one or two Gaussian functions) and for the remaining background which consists notably of the correlated lepton pairs from open-charm and Drell-Yan production.

Figure 4 shows the background subtracted di-lepton invariant mass distributions measured in the central arm (left) and in the muon arms (right) for $p + p$ collisions at $\sqrt{s} = 200$ GeV during the 2005 data taking period.

The J/ψ invariant yield in a given transverse momentum and rapidity bin is:

$$\frac{B_{ll}}{2\pi p_{\mathrm{T}}} \frac{d^2 N_{\mathrm{J}/\psi}}{dp_{\mathrm{T}} dy} = \frac{1}{2\pi p_{\mathrm{T}}} \frac{N_{\mathrm{J}/\psi}}{N_{evt} \Delta y \Delta p_{\mathrm{T}} A\varepsilon} \tag{1}$$

with B_{ll} being the branching ratio for J/$\psi \to l^+ l^-$ (~ 6 %); $N_{\mathrm{J}/\psi}$ the number of J/ψ measured in the bin; N_{evt} the corresponding number of events; Δy the rapidity range; Δp_{T} the transverse momentum range and $A\varepsilon$ the acceptance and efficiency correction for J/ψ. This correction is evaluated using PYTHIA to simulate J/ψ, GEANT to propagate the generated particles through the detector and calculate their energy deposit and multiple scattering, and PHENIX simulation and reconstruction software to model the detector performances and reconstruct the particles trajectory and momentum. To account for the detector occupancy, the simulated events are embedded in real data events prior to the reconstruction. The resulting embedded events are reconstructed using the same algorithm and the same analysis cuts as the real data.

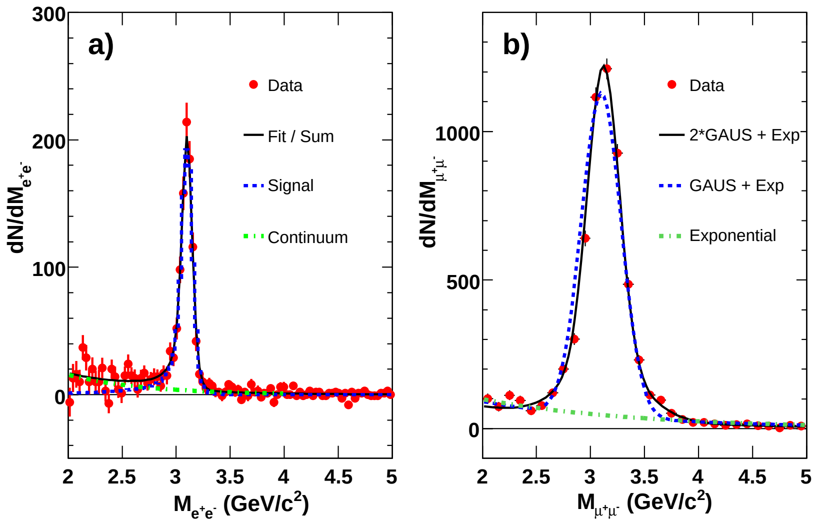

Figure 4: Left (right) panel: Di-electrons (di-muons) invariant mass distribution measured in the PHENIX central (muon) spectrometer for $p+p$ collisions at $\sqrt{s} = 200$ GeV during the 2005 data taking period.

6 Results in $p+p$ collisions

The J/ψ production cross-section in $p+p$ collisions is obtained by multiplying the invariant yield of equation 1 by the total $p+p$ inelastic cross-section:

$$\frac{d^2\sigma_{\mathrm{J}/\psi}}{dp_{\mathrm{T}}dy} = \frac{d^2 N_{\mathrm{J}/\psi}}{dp_{\mathrm{T}}dy}\sigma_{pp}^{inel} \tag{2}$$

Figure 5 shows the J/ψ production cross-section as a function of the J/ψ rapidity in $p+p$ collisions at $\sqrt{s} = 200$ GeV. The squares correspond to the central arm measurements and the circles to the muon arms measurements. The values are fitted with several line shapes originating either from models of the J/ψ production or from empirical functions. Each fit function is integrated and the average of the integrals is used to compute the total J/ψ production cross-section times branching ratio $B_{ll}\sigma_{pp}^{J/\psi} = 178{\pm}3{\pm}53{\pm}18$ nb.

PHENIX also measured the transverse momentum dependence of the J/ψ production. It is used to calculate the J/ψ mean square transverse momentum $\langle {p_{\mathrm{T}}}^2 \rangle$ and compare it to the results obtained by past experiments at different energies.

These are the latest results published by the PHENIX experiment for $p+p$ collisions and represent a factor 10 increase in the statistics with respect to earlier results published in 2003 [4]. More $p+p$ data have been taken in 2006 with an additional factor 3 increase but they have not been analysed yet.

Our group took a leading role in estimating the acceptance and efficiency corrections entering the denominator of the J/ψ production invariant cross-section (equation 1), using the same techniques as for the Au + Au analysis. It also participated to the PHENIX internal committee (of about 10 scientists) responsible for the writing of the final publication that present the results to the scientific community [5].

7 Results in d + Au collisions

J/ψ production in d + Au collisions at $\sqrt{s_{\mathrm{NN}}} = 200$ GeV has been measured by the PHENIX collaboration during the 2003 data taking period. The published results [4] are used to evaluate the so called cold nuclear

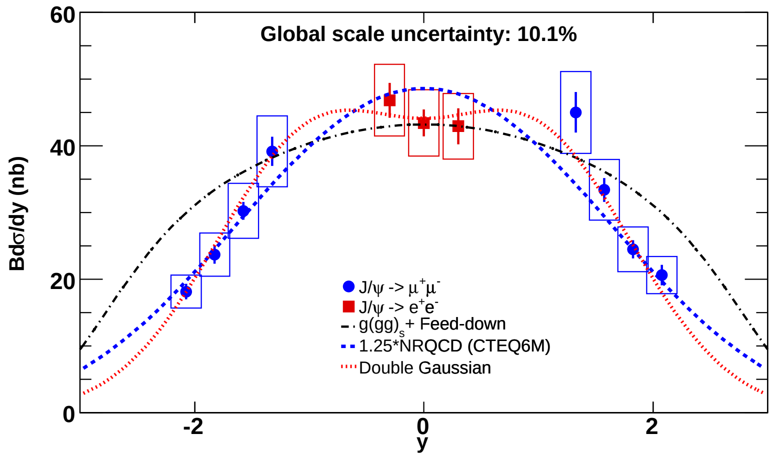

Figure 5: J/ψ production invariant cross-section as a function of the J/ψ rapidity y in $p+p$ collisions at $\sqrt{s} = 200$ GeV.

effects that affect the J/ψ production beyond that measured in $p+p$ collisions and without formation of the QGP. Such effects are:

- shadowing and anti-shadowing effects [6] which characterize how the distribution functions of a parton inside a nucleon are modified by the presence of the surrounding nucleons inside a nucleus;
- the Cronin effect [7] which characterizes elastic scattering of the initial gluons in the nucleus, thus modifying the resulting J/ψ transverse momentum distribution;
- J/ψ interaction with hadronic co-movers and nuclear absorption.

7.1 Rapidity and centrality dependence of the nuclear modification factor

The nuclear modification factor is used to compare the J/ψ production in a given type of nucleus-nucleus (A+B) collisions to what would be expected from $p+p$ collisions. For a given centrality, transverse momentum and rapidity bin, it is:

$$R_{\mathrm{AB}} = \frac{dN^{\mathrm{AB}}_{\mathrm{J}/\psi}/dp_{\mathrm{T}}dy}{N_{\mathrm{coll}}dN^{\mathrm{pp}}_{\mathrm{J}/\psi}/dp_{\mathrm{T}}dy} \tag{3}$$

with $dN^{\mathrm{AB}}_{\mathrm{J}/\psi}/dp_{\mathrm{T}}dy$ the J/ψ yield measured in A+B (here $\mathrm{d}+\mathrm{Au}$) collisions; $dN^{\mathrm{pp}}_{\mathrm{J}/\psi}/dp_{\mathrm{T}}dy$ the J/ψ yield measured in $p+p$ collisions and N_{coll} the number of nucleon-nucleon collisions geometrically corresponding to one A+B collision in the considered centrality bin, evaluated using simulations based on a Glauber model of the nucleus.

Figure 6(a) shows the J/ψ nuclear modification factor as a function of the J/ψ rapidity for $\mathrm{d}+\mathrm{Au}$ collisions at $\sqrt{s_{\mathrm{NN}}} = 200$ GeV. J/ψ produced at positive rapidity correspond to gluons with small x_{Au}, the fraction of the nucleon momentum that is carried by the gluon in the Au nucleus. On the contrary, J/ψ produced at negative rapidity correspond to gluons with large x_{Au}. The J/ψ production appears to be slightly reduced at positive rapidity (small x_{Au}) and slightly enhanced at negative rapidity (large x_{Au}). This trend is reproduced by several parametrizations of the nuclear shadowing represented in Figure 6(a). A J/ψ nuclear absorption cross-section of 1 to 3 mb must be added to the shadowing/anti-shadowing effects in order to reproduce the overall magnitude of the measured R_{dA}.

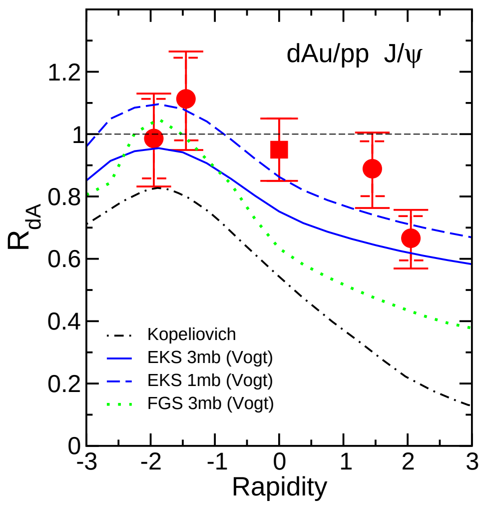

(a)

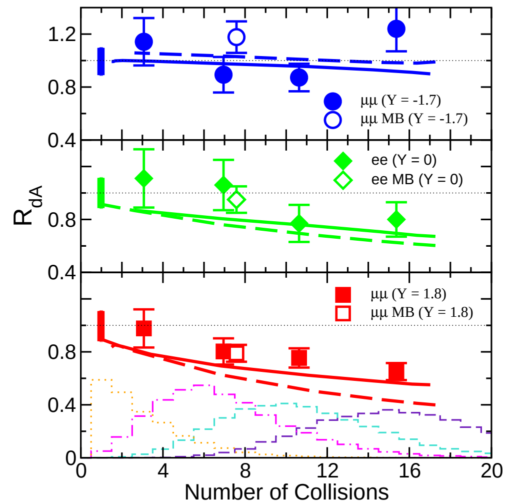

(b)

Figure 6: Left: J/ψ nuclear modification factor R_{dA} as a function of the J/ψ rapidity in $\mathrm{d}+\mathrm{Au}$ collisions at $\sqrt{s_{\mathrm{NN}}} = 200$ GeV. Right: J/ψ nuclear modification factor R_{dA} as a function of the number of nucleon-nucleon collisions.

Figure 6(b) shows the J/ψ nuclear modification factor as a function of N_{coll} for 3 rapidity bins. The top and bottom panels correspond to PHENIX muon arms measurement whereas the middle panel corresponds to PHENIX central arm.

For peripheral collisions (small values of N_{coll}) the nuclear modification factor is close to 1. For increasing values of N_{coll}, there is little dependency of the R_{AA} at negative rapidity and a decrease of the R_{AA} at mid and positive rapidity. The lines represent the expected R_{AA} when using two different parametrizations of the shadowing.

7.2 Extrapolation to $\mathrm{Au}+\mathrm{Au}$ measurements

The results obtained in $\mathrm{d}+\mathrm{Au}$ collisions are used to evaluate nuclear matter effects that affect the J/ψ production in absence of the QGP. They must be carefully extrapolated to the $\mathrm{Au}+\mathrm{Au}$ case to determine if any additional (anomalous) J/ψ suppression is observed. Two approaches have been used so far to perform this extrapolation.

The first approach [8] uses the parametrization of the gluon distribution functions in the Au nucleus and the nuclear absorption cross-section that match the measured R_{dA} best (Figure 6(a)) as an input to a model of $\mathrm{Au}+\mathrm{Au}$ collisions.

The second approach [9] uses the measured R_{dA} as a function of the J/ψ rapidity and N_{coll} (Figure 6(b)) as an input to a Monte Carlo simulation of each $\mathrm{Au}+\mathrm{Au}$ collision. For each nucleon-nucleon collision that occurs in a $\mathrm{Au}+\mathrm{Au}$ collision at a given impact parameter b_{AA}, the impact parameter of each nucleon with respect to the other Au nucleus b_i is evaluated as well as the corresponding R_{dA}. Both found R_{dA} are then combined to estimate the J/ψ survival probability:

$$R_{\mathrm{AA}}(y, b_{\mathrm{AA}}) = \sum_{1}^{N_{\mathrm{coll}}} \left(R_{\mathrm{dA}}(-y, b_1) R_{\mathrm{dA}}(y, b_2)\right) / N_{\mathrm{coll}} \tag{4}$$

This method has the advantage of being less model dependent than the first and allows a more precise accounting for the experimental errors on the R_{dA} measurement.

Results obtained with these two approaches are shown in Figure 7.

8 Results in Au + Au collisions

The top panel of Figure 7 shows the J/ψ nuclear modification factor R_{AA} as a function of the number of participant nucleons N_{part} in Au + Au collisions at $\sqrt{s_{\mathrm{NN}}} = 200$ GeV measured by the PHENIX experiment in 2004. The open circles correspond to the central arm measurement at mid rapidity and the full circles to the muon arms measurement at forward rapidity. The lines are predicted cold nuclear matter effects at mid and forward rapidity extrapolated from d + Au measurements as described in the previous section. The shaded areas correspond to the error associated to the second method. The errors associated to the first method are not available but should be of about the same magnitude.

The nuclear modification factor is close to 1 for peripheral collisions (small values of N_{part}) and decreases both at forward and mid rapidity when N_{part} increases. This is the first measurement of a J/ψ suppression in Au + Au collisions at this energy. For central events, R_{AA} is about 0.3 (0.2) at mid (forward) rapidity and the suppression is larger than the one expected from cold nuclear effects, although these expectations suffer from large uncertainties.

The bottom panel of Figure 7 shows the ratio between the J/ψ R_{AA} measured at forward rapidity and the J/ψ R_{AA} measured at mid rapidity. This ratio is compatible with 1 for peripheral collisions. It then decreases and reaches a plateau of about 0.6 for $N_{\mathrm{part}} > 100$, meaning that there is more suppression at forward rapidity than at mid rapidity.

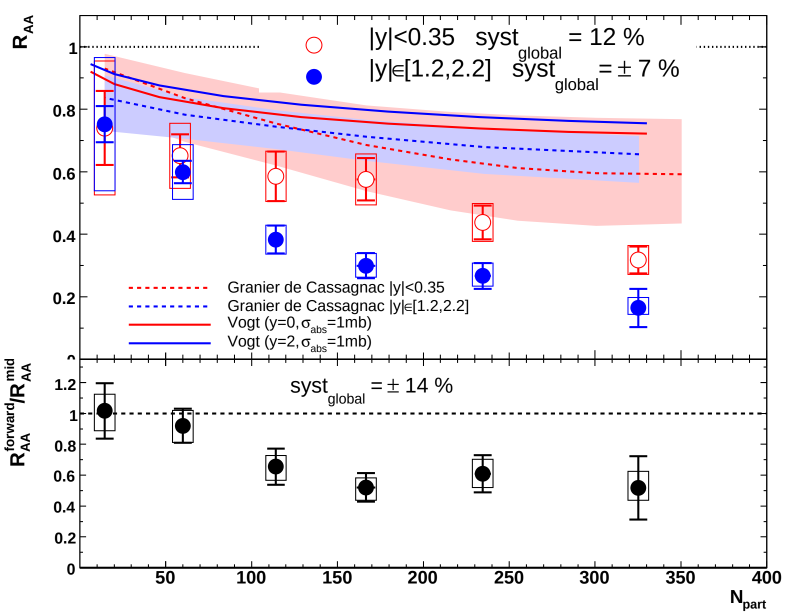

Figure 7: Top: J/ψ nuclear modification factor R_{AA} as a function of the number of participant nucleons N_{part} in Au + Au collisions at $\sqrt{s_{\mathrm{NN}}} = 200$ GeV. Bottom: ratio between the J/ψ R_{AA} measured at forward and the R_{AA} measured at mid rapidity as a function of N_{part}.

Figure 8 shows the J/ψ nuclear modification factor R_{AA} as a function of the J/ψ transverse momentum (left panel) and rapidity (right panel) for 4 centrality bins in Au + Au collisions at $\sqrt{s_{\mathrm{NN}}} = 200$ GeV. These measurements are used to determine how the J/ψ transverse momentum and rapidity distributions are affected by the collision centrality. Within the large error bars, the transverse momentum distribution shows little dependency on centrality at both forward and mid rapidity. On the other hand, the rapidity distribution tends to get slightly narrower for more central collisions. These distributions provide an important constraints on models that aim to describe the J/ψ production in Au + Au collisions with or without formation of the QGP.

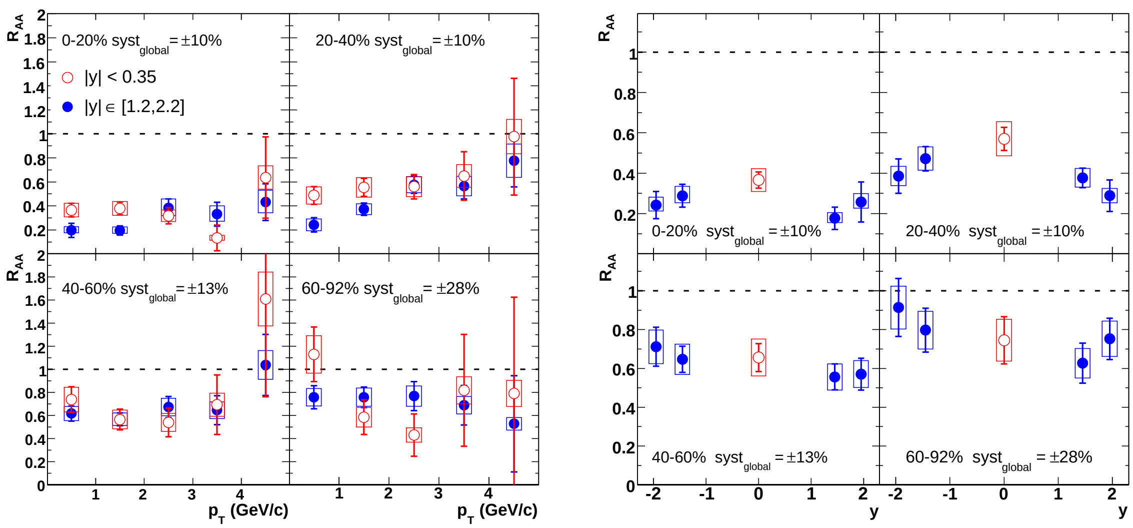

(a) (b)

Figure 8: J/ψ nuclear modification factor R_{AA} as a function of the J/ψ transverse momentum (left) and rapidity (right) for 4 centrality bins in Au + Au collisions at $\sqrt{s_{\mathrm{NN}}} = 200$ GeV.

As for the 2005 $p + p$ analysis, our group took a leading role in estimating the acceptance and efficiency corrections that enter the denominator of the J/ψ production invariant yield (equation 1) and in evaluating the number of measured J/ψ for each centrality, rapidity and transverse momentum bin. The accuracy of these estimates directly affects the quality of the final results. We were also responsible for the development and use of an additional offline trigger algorithm that rapidly selects events containing a J/ψ candidate prior to the full reconstruction. We presented the preliminary J/ψ results in Au + Au collisions at the 2005 Quark Matter international conference for the PHENIX collaboration and chaired the PHENIX internal committee responsible for the writing of the final publication that present the results to the scientific community [10].

9 Interpretation

A significant J/ψ suppression relative to N_{coll} scaling of proton-proton cross-section is observed for central Au + Au collisions at RHIC at both forward and mid rapidity. It exceeds the suppression expected by extrapolating the cold nuclear matter effects measured in d + Au collisions, although the uncertainty on the latter is large. At mid rapidity, the magnitude of the suppression is found similar to that observed at the SPS [11] at a smaller $\sqrt{s_{\mathrm{NN}}}$, whereas models able to reproduce the SPS data would predict a larger suppression due to the increased energy density of the created medium. For the same reason such models would predict a larger suppression at mid rapidity than at forward rapidity, which is also contradicted by the data. Additional mechanisms are proposed that suggest a regeneration of the J/ψ (on top of the suppression due to colour screening) via the recombination (coalescence) of charm quarks produced in two different partonic interactions. Such predictions rely heavily on the open charm production cross-section in Au + Au collisions, which is still largely unknown. They usually apply to mid-rapidity data only and it is unclear today if they are able to reproduce the trend of the suppression as a function of N_{part}. This is even more true when considering the rapidity and transverse momentum dependence of the suppression, as shown in Figure 8.

10 Perspectives

Starting from 2007 the group took the responsibility of the simulation software for the whole PHENIX spectrometer (as opposed to the muon arms only). This consists in providing the proper simulations needed to estimate the detector acceptance and efficiency as well as the physical and combinatorial background specific to the various analysis performed by the collaboration, such as high transverse momentum particle correlations, light and heavy particle elliptic flow measurements, single muons and single electrons productions (related to open charm production).

The 2007 data taking period will consist again of Au + Au collisions with an expected integrated luminosity four times larger than in 2004. This will result in more accurate measurements, a better control of the systematic errors and possibly new measurements such as the J/ψ elliptic flow. More data will also be taken using d + Au collisions to have a better control on cold nuclear matter effects that need to be subtracted from the suppression observed in heavy ion collisions. This should occur in 2008 or 2009. Finally, PHENIX plans several detector and electronics upgrades to cope with the RHIC luminosity upgrade foreseen in 2010. So far no contribution from the DAPNIA to these upgrades is envisaged.

References

[1] T. Matsui and H. Satz. J/ψ suppression by quark-gluon plasma formation. *Phys. Lett.*, B178:416, 1986.

[2] Frithjof Karsch. Lattice QCD at high temperature and density. *Lect. Notes Phys.*, 583:209–249, 2002.

[3] K. Adcox et al. Phenix detector overview. *Nucl. Instrum. Meth.*, A499:469–479, 2003.

[4] S. S. Adler et al. J/ψ production and nuclear effects for d+Au and p+p collisions at $\sqrt{s_{\rm NN}} = 200$ GeV. *Phys. Rev. Lett.*, 96:012304, 2006.

[5] A. Adare et al. J/ψ production vs transverse momentum and rapidity in p+p collisions at $\sqrt{s_{\rm NN}} =$ 200 GeV. 2006, hep-ex/0611020.

[6] A. Accardi et al. Hard probes in heavy ion collisions at the LHC: PDFs, shadowing and pA collisions. 2003, hep-ph/0308248.

[7] Alberto Accardi. Cronin effect in proton nucleus collisions: A survey of theoretical models. 2002, hep-ph/0212148.

[8] R. Vogt. Baseline cold matter effects on j/psi production in AA collisions. 2005, nucl-th/0507027.

[9] Raphael Granier de Cassagnac. A d+Au data-driven prediction of cold nuclear matter effects on J/ψ production in Au+Au collisions at RHIC. 2007, hep-ph/0701222.

[10] A. Adare et al. J/psi production vs centrality, transverse momentum, and rapidity in Au+Au collisions at $\sqrt{s_{\rm NN}} = 200$ GeV. 2006, nucl-ex/0611020.

[11] B. Alessandro et al. A new measurement of J/ψ suppression in pb-pb collisions at 158-GeV per nucleon. *Eur. Phys. J.*, C39:335–345, 2005.